doi:10.20944/preprints201808.0203.v1

Synthesis of Cu,N-Doped TiO_2 Nanotube and Study on Photoelectric Properties

Yiming Liu [1,2], Yanhao Sun [1] , Zhuobin Yu[1], Wanggang Zhang[1*], Peide Han[,1*,]
[1] College of Materials Science and Engineering, Taiyuan University of Technology,
Taiyuan Shanxi 030024, China
[2] Shanxi Academy of Analytical Sciences, Taiyuan Shanxi 030006, China

Abstract: Cu,N-TiO_2 nanotube (Cu,N-TNT) is prepared through a novel magnetron sputtering and anodic oxidation method. Then the morphology, structure and physicochemical property of Cu,N-TNT was analyzed by XRD, SEM, TEM, EDX and UV-vis-DR. The results indicate that the evenly doped copper is beneficial to the transformation of the TNT from anatase to rutile and play a key role in the morphology of the Cu,N-TNT. The doped Cu and N in the TNT influence the growth orientation of the TiO_2 crystals, which result in the lattice distortion and wider the interplanar spacing 60s-Cu,N-TNT has less band gap and stronger absorption intensity in visible region than other Cu,N-TNT samples, which make the combination rate of photogenerated electron and photogenerated hole decrease greatly, thus beneficial to its physicochemical property.

Key words: Titanium dioxide nanotube, photoelectric properties, co-doping, magnetron sputtering

1. Introduction

Owing to its cheap, non-toxic and high stability proprieties, TiO_2 has been regarded as an important semiconductor nanometer material and could be applied in the field of solar cell, photocatalyst, gas sensor, etc[1-7]. However, the shortcomings of its wide band gap and the fast recombination of the photogenerated electron–hole pairs greatly restricted its practical application[8, 9]. To overcome the shortcomings,

---

Corresponding author: Peide Han, professor. Email: hanpeide@tyut.edu. cn;

Corresponding author: Wanggang Zhang, Doctor. Email: zwgang0117@163.com;

intensive efforts such as implanting an adequate amount of cation or anion and the doping of nonmetallic or metallic elements had been made to extend the work spectrum of TiO_2 to the visible (VIS) regions, and to enhance the electron–hole separation [10-13]. At present, it is demonstrated that metal ions are used as dopants can enhance remarkably photocatalytic activity and strong absorption in visible light regions[14, 15]. Moreover, as an low-cost and abundant metal, copper have tremendous potential in doping for TiO_2[16] . However, to our knowledge, single Cu ion doping has limited improvement in the visible light absorption efficiency and can not meet the needs of practical application of the nanotubes[17, 18]. Furthermore, it is said that TiO_2 modified by nonmetal (such as N, F and S) could narrow the band gap and inhibit the indirect recombination of photogenerated electrons and holes[19-21]. Therefore, it is necessary to implant simultaneous two kinds of atoms into TiO_2.

So far, many kinds of preparing methods such as ion injection, chemical vaporous deposition and heat-treating process have been used to modify metal ions in TiO_2. However, the preparation procedure of these method are usually complicated and the doping amount is relatively low. Furthermore, these solution-based methods can lead to secondary pollution and influence on the morphology of nanotube[22-25]. On the contrary, the samples prepared by magnetron sputtering have the advantage of composition and thickness uniformity, while the preparation of nanotubes by anodic oxidation is simple and have good repeatability[26-28]. Therefore, magnetron sputtering and anodic oxidation was used in this paper to prepare Cu,N-TiO_2, where the doping amount of Cu can easily be controlled by the sputtering time and N can be doped into the nanotubes by changing the sputtering atmosphere. Furthermore, the photoelectric property of the co-doped TiO_2 nanotube arrays were also studied.

2. Experimental

2.1 Preparation of Cu,N-Ti nanofilms

Cu (99.9 wt.%) and Ti target (99.9 wt.%) targets were used to prepare Cu,N-Ti nanofilms on titanium sheets at room temperature (25°C) by magnetron sputtering in a multifunctional magnetron sputtering instrument (JGP560B). Firstly, titanium sheet (30×10×0.1 mm) were ultrasonically cleaned with acetone, ethyl alcohol, and deionized water in sequence, respectively, and then is baked at 105 ℃. Secondly, the mixed gas (the flow rate of $Ar:N_2=70:1$) was flowed into the sputtering chamber when the pressure of the sputtering chamber reached to 8×10^{-4} Pa. The titanium sheets were pre-puttered for 2 min in order to remove metal oxides and other impurities. The distance between the specimen and the target material is about 30 mm, and the chamber pressure was 1 Pa during sputtering. The thickness of Cu, N-Ti nanofilms was controlled by the power and time of sputtering. The 2 μm Cu,N-TiO_2 nanofilms were generated using Ti and Cu target by alternately sputtering. In the process, the total sputtering time of Ti target is 1 hour while the sputtering time of Cu target vary from 20s, 40s, 60s, 80s, and 100s. The Cu,N-Ti nanofilms were calcined in Ar at 450 ℃ for 2 h with a heating rate of 2 ℃/min .

2.2 Preparation of Cu,N-TiO_2 nanotubes

The above Cu,N-Ti nanofilms and a platinum foil was used as the working electrode and the counter electrode in the electrolyte of a mixture including water, ethylene glycol and 0.02 M NH_4F at 25 ℃, respectively. The samples that were generated when the anodization voltage was 30 V, and the anodization time was 45 minutes at 25 ℃ were ultrasonically cleaned with deionized water. The Cu,N-TiO_2 nanotubes were calcined in Ar at 450 ℃ for 2 h with a heating rate of 2 ℃/min .

2.3 Materials characterization

The morphology and selected area electron diffraction (SAED) patterns of the prepared samples were examined using field emission scanning electron microscopy (FESEM) (Tescan MIRA3 LMH) at 10 kV and transmission electron microscopy (TEM) (JEOL JEM 2100F) at 200 kV. The composition of the prepared samples was determined using energy dispersive spectroscopy (EDS) (OXFORD X-Max 80), and the crystal structure of the prepared structures was analyzed with Cu Kα radiation on a Rigaku D/max 2500 X-ray diffractometer with patterns recorded in a range of

20–80° (Rigaku Smart Lab). Optical absorption of the Cu,N-TNT in the wavelength range of 300–800 nm was measured using a UV-vis spectrophotometer (HITACHI: U-3900). The binding energy was determined using X-ray photoelectron spectroscopy (XPS) (Escalab 250).

2.4 Photoelectrochemical activity

Photoelectrochemical activity of the prepared TiO_2 nanotubes (or modified TNT) was carried out in a three-electrode cell. The prepared TNT or modified TNT , Pt foil, and SCE (saturated calomel electrode) act as working, counter, and reference electrodes in 0.5 M Na_2SO_4 electrolyte, respectively. A 500 W Xenon lamp (TrustTech, Beijing, China) with a cut off filter ($\lambda > 420$ nm) was used as the light source. The photocurrent was conducted by a CHI660D electrochemical workstation.

3. Results and discussion

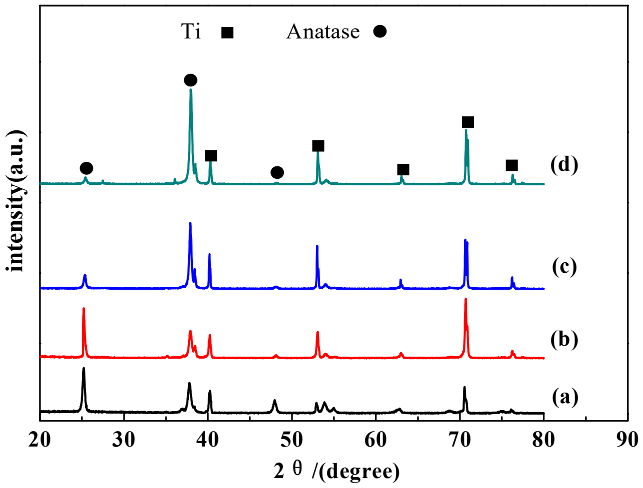

Fig. 1 XRD patterns of the prepared TiO_2 nanotubes (a)TNT; (b)N-TNT; (c)60s-Cu-TNT; (d)60s-Cu,N-TNT

X-ray diffraction (XRD) was carried out on TiO_2 nanotubes, N doped TiO_2 nanotubes Cu 60 s doped TiO_2 nanotubes and N-Cu 60s co-doped TiO_2 nanotubes, which are referred to as TNT, N-TNT, 60s-Cu-TNT and 60s-Cu,N-TNT, respectively to confirm their phase structure and crystal transformation. Fig. 1 shows the XRD patterns of the nanotubes calcined at 450 ℃. It is obviously observed that all the nanotubes clearly display the peaks of TiO_2, including the planes of (101), (004) and (200) at 2θ values of ca. 25.3°, 37.9° and 48.2°, respectively (JCPDS No.21-1272). However, for the 60s-Cu,N-TNT, two new peaks centered at 27.4° and 36.1°, which belongs to (110) and (101) planes of rutile TiO_2 (JCPDS No.21-1276) appears. In general, it is widely known that it could not be observed the diffraction characteristic peaks of rutile TiO_2 when TNT were calcined at 450℃[29, 30]. However, it occurs the diffraction characteristic peaks of rutile TiO_2 when TNT doped with Cu and N simultaneously were calcined at 450 ℃. The results demonstrate that Cu,N co-doping promote the phase transition from anatate to rutile of TiO_2, which should result from decreasing the transition temperature from anatate to rutile of TiO_2 according to reported literatures[31]. Furthermore, it is observed that besides the peaks belongs to anatase and rutile of TiO_2, titanium diffraction peaks can also be detected, but no peaks belongs to copper or copper oxide appears, demonstrating that the Cu element may be exist in the form of ions. At the same time, it is found there is similar grain growth orientation among Cu,N-TNTs that the intensity of (101) plane of anatate TiO_2 become weaker and the intensity of (004) plane of anatate TiO_2 become stronger with increasing the sputtering time of Cu for Cu,N-TNT samples in Fig.S1. The results indicate that Cu,N-TNT with increasing copper content promote the optimal growth of anatase (004) plane.

The morphological features of the prepared nanotubes were investigated using FESEM. Fig.2 (a) and (b) show the top-view and side-view of the TNT. It is presented that TNT had a complete nanotube arrays structure, whose average length, diameter and thickness is 2 μm, 50 nm, and 15 nm, respectively. From the topology images of Fig. 2 (c)-(h), it is observed that the tube diameter and tube length changed little after N or Cu doping, confirming that Cu or N doping has little effect on the morphology of the nanotubes. Furthermore, in the Cu doped nanotubes, no copper or copper oxide nanoparticles can be observed, further demonstrating that the Cu element maybe exist in the form of ions, and consist with our XRD results. Interestingly, when more Cu added in the N-nanotubes, the tubular structure collapses and cannot be maintained after annealing at 450 ℃, which confirms buy the SEM images in Fig.S2, meaning that TNT nanobutes were destroyed with the increase of Cu content in Cu,N-TNT samples. The above phenomena could result from that excess copper content for Cu,N-TNT samples inhibits the generation of nanotubes during the anodic oxidation process.

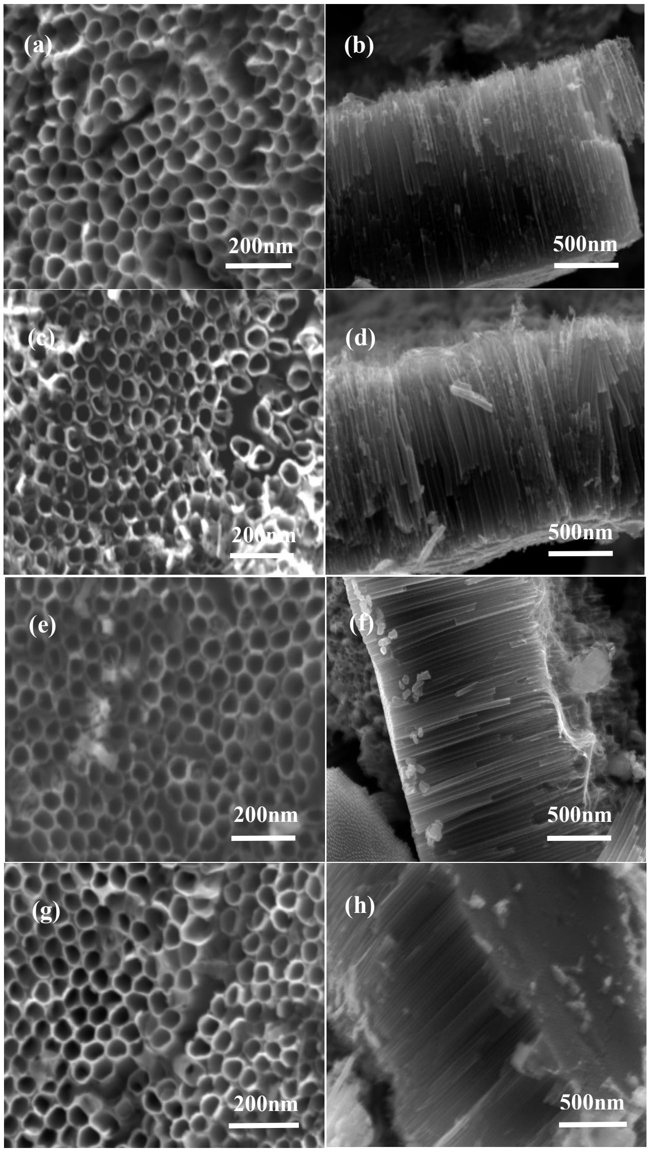

Fig. 2 SEM images of the TiO_2 nanotubes arrays; (a) overview of TNT; (b) side view of TNT; (c) overview of N-TNT; (d) side view of N-TNT; (e) overview of Cu-TNT; (f) side view of Cu-TNT; (g) overview of Cu, N-TNT; (h) side view of Cu, N-TNT

Further analysis the morphology difference of the nanotubes after Cu or N doping, the morphological features of the prepared nanotubes have been investigated using TEM. Fig. 3a to h show the TEM and HRTEM images TNT, N-TNT, Cu-TNT and Cu,N-TNT, respectively. It is found from Fig. 3a and c that there is no observable change in the morphology of the nanotubes after N doping. Figs. 3b and d are high-resolution TEM (HRTEM) image of TNT and N-TNT, which both show the characteristic lattice fringe of 3.52 Å for TiO_2 nanotubes, corresponding to the (101) plane of anatase TiO_2. Such a result is consistent with the presence of anatase TiO_2 as observed from the XRD patterns in Fig. 1. However, for the N-TNT in Fig.3 d, an obvious lattice expansion could be observed, and the lattice spacing 3.68 Å also belongs to (110) planes of anatase TiO_2 which should attributed that TNT is modified by copper and is accordance with reported literature[32, 33].

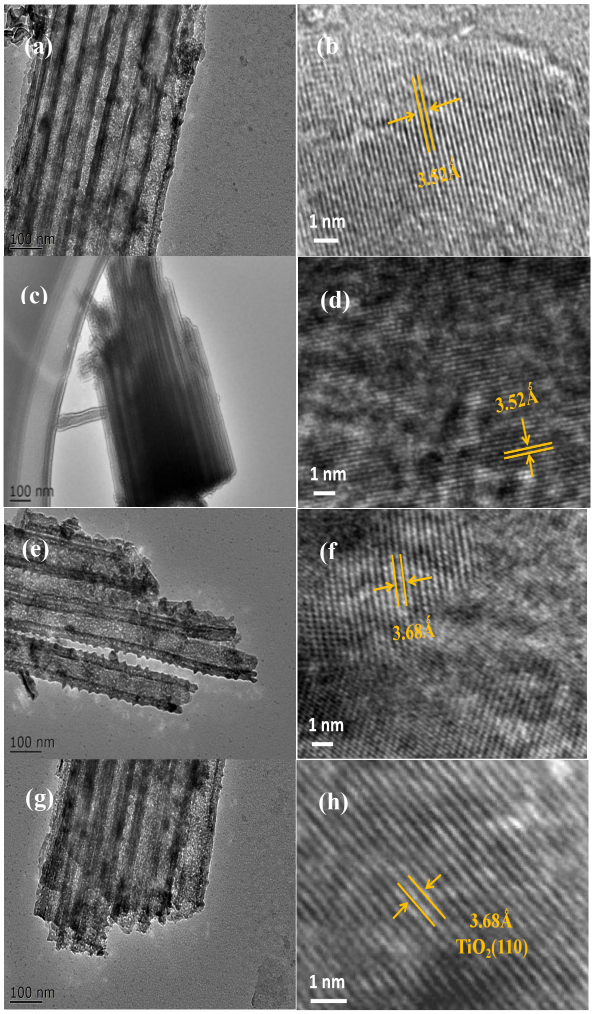

Fig. 3 (a) TEM image of TNT; (b) HRTEM image of TNT; (c) TEM image of N-TNT; (d) HRTEM image of N-TNT; (e) TEM image of Cu-TNT; (f) HRTEM image of Cu-TNT; (g) TEM image of Cu,N-TNT; (h) HRTEM image of Cu,N-TNT

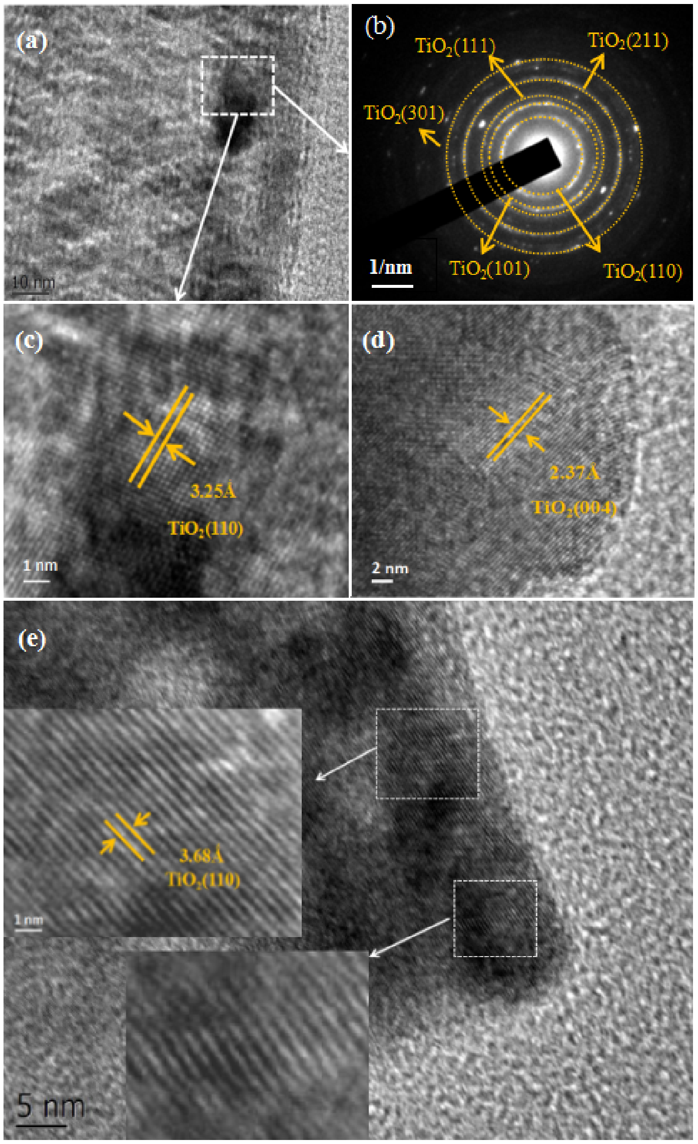

Fig. 4 (a) HRTEM image of 60s-Cu,N-TNT; (b) The Regional diffraction patterns of Rutile; (c) HRTEM image of Rutile; (d) (004) crystal plane of Anatate; (e) Anatase crystal plane with lattice distortion.

The special selected HRTEM and SADP of 60s-Cu,N-TNT were separately listed in Fig. 4. The diffraction pattern of the selected region is listed in Fig.4 (b) that is consistent with rutile TiO_2 and the lattice distance is 3.52 Å that agrees with (110) planes of rutile TiO_2, which suggest that 60s-Cu,N-TNT contains rutile phase composition and is identical with the results in Fig.1. Meantime, it is observed that the lattice space is 2.37 Å that agrees with (004) plane of anatase TiO_2 and there is a large area of (004) plane in Fig.4 (d), which indicated that promoted the optimal growth of (004) crystal plane among TNT and modified samples [33-35]. Furthermore, there are obviously lattice distorted in Fig.4 (e), whose reason should be attributed to that Cu and N is incorporated into the lattice of TNT. The results indicate that TNT have been modified simultaneous by Cu and N.

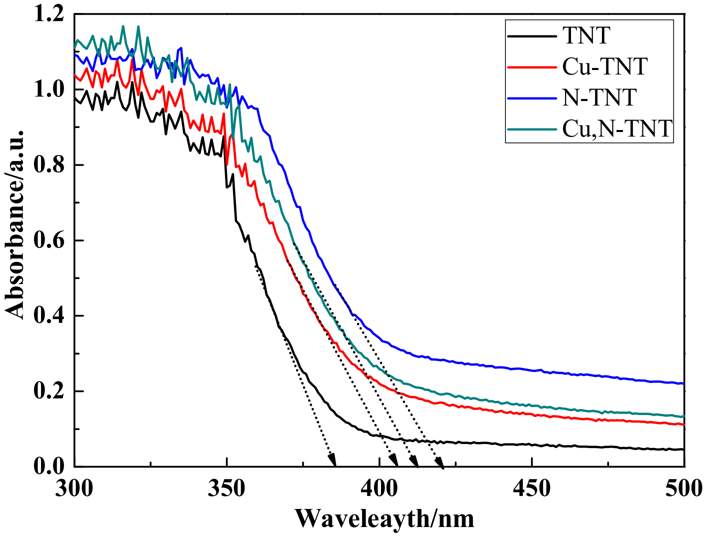

Fig. 5 UV-Vis spectrum of TNT; 60s-Cu-TNT; N-TNT; 60s-Cu,N-TNT

The UV-Vis spectra of TNT, 60s-Cu-TNT, N-TNT, 60s-Cu,N-TNT is listed in Fig.5. It is found that the absorption edge of TNT is ~387 nm, and the absorption peak generates bathochromic shift in ultraviolet visible absorption spectrum. The absorption edge follows in the order of TNT< Cu-TNT < N-TNT< 60s-Cu,N-TNT. The band gap of 60s-Cu,N-TNT is 2.93eV, which has a 0.27 eV shift than that of TNT, whose band gap is 3.2 eV when calculating from the equation: $(ahv)^2= k(hv-Eg)$ (a: absorption coefficient, h: Planck constant, v: light frequency, Eg: band energy)[36, 37]. The results indicate it is an effective method to decrease the band gap of TNT and increase the absorption intensity in visible region after Cu and nitrogen element doped. The above phenomena could put down to that the crystal structure of TiO_2 is destroyed to form impurity level between conduction band and valence band in the process of TNT doped with Cu and N, which could prevent photogenerated-electron and photogenerated-hole recombine and result in less band gap and stronger absorption intensity in visible spectra[38]. Therefore, the Cu,N-TNT film was further are studied in detail.

The EDS analysis for section graphs of 60s-Cu,N-TNT is shown in Fig.S3. The results indicate that the major ingredient of 60s-Cu,N-TNT is Ti and O, and while the content of evenly distributed copper and evenly distributed nitrogen is 1.0 at.% Cu and 5.1 at.% N, which ascertain that TNT was successfully modified by Cu and N element.

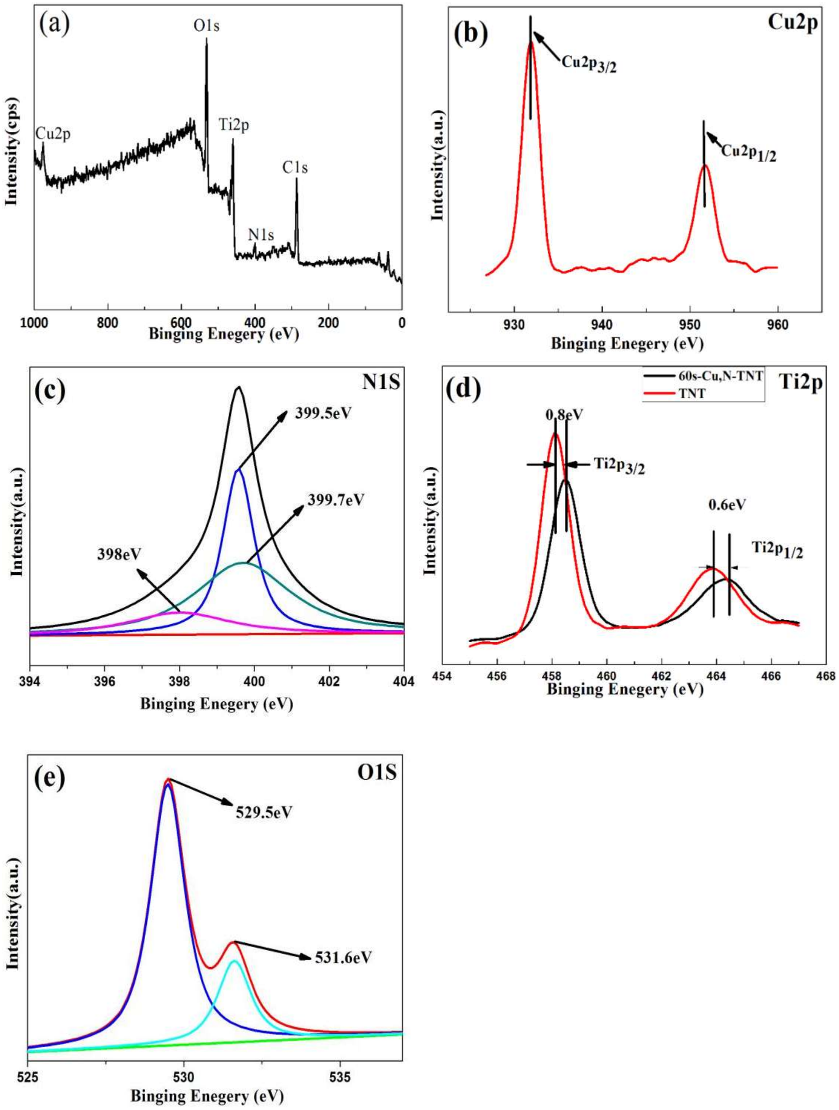

Fig. 6 XPS spectra of 60s-Cu-TNT (a)Full spectrum diagram of 60s-Cu-TNT; (b)Cu2p; (c)N1s; (d)Ti2p; (e)O1s

XPS spectra were measured to further investigate the chemical bonding state through of the elements. Figure 6(a) shows a general scan spectrum of XPS over a large energy range at low resolution of the prepared 60s-Cu-TNT. It is evident that the 60s-Cu,N-TNT is composed of Ti, O, N, C and Cu elements , which is consistent with EDS results in the supporting information in Fig.S3. Trace amounts of C is attribute to the accidental hydrocarbon in the XPS instrument itself or the adventitious carbon-based contaminant. The binding energy of $Cu2p_{3/2}$ and $Cu2p_{1/2}$ in Fig. 6(b) is 932.0 eV and 952.2 eV, which should be attributed to that Cu exist as either Cu^{2+} or Cu^{+}[39] . The N1s at 399.8 eV and 399.5 eV are assigned to Ti-O-N bond while the N1s at 398.0 eV correspond to Ti-N bond[39, 40]. The binding energy of $Ti2p_{3/2}$ and $Ti2p_{1/2}$ in Fig. 6(d) are 463.6 eV and 458.0 eV that should be assigned to Ti^{4+} in TiO_2 bond for 60s-Cu,N-TNT, which is more negative than that of $Ti2p_{3/2}$ and $Ti2p_{1/2}$ for TNT. Likewise, the O1s at 531.6 eV for 60s-Cu,N-TNT could belong to Cu-O bond, and the O1s at 529.2 eV for 60s-Cu,N-TNT is more negative than the O1s at 530.0 eV for TNT. The reason should result from synergy between Ti-N-Ti bond and TNT modified by Cu[40].

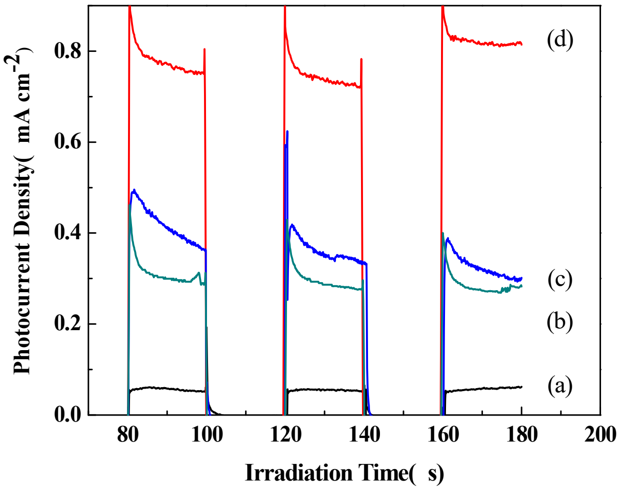

Fig. 7 Transient photoelectric response maps of (a)TNT; (b)N-TNT; (c)60s-Cu-TNT; (d)60s-Cu,N-TNT

A set of photoelectrochemical (PEC) measurements were conducted in a 0.5 M Na_2SO_4 solution to evaluate the photoelectrochemical (PEC) properties of TNT and modified TNT under visible light radiation, which is presented in Fig.6. It is observed that Cu,N-TNT electrode has the better sensitivity than TNT, Cu-TNT, and N-TNT electrodes, which could be attributed to that the 60s-Cu,N-TNT has the less band gap than TNT, N-TNT and Cu-TNT in Fig.8. The results suggest that TNT implanted Cu and N element can improve obviously the responsivity to visible light, and may be used as promising photo-anode. There are two main reasons:(1)TNT was modified by N may generate a new N 2p orbital band above the O 2p valence band, which makes the band gap become less[41]. (2)The crystal structure was destroyed when metal ions doped into the TiO_2 lattice and metal ions could capture photoelectron or hole to decrease the recombination rate of photo-electron and photo-hole[42].

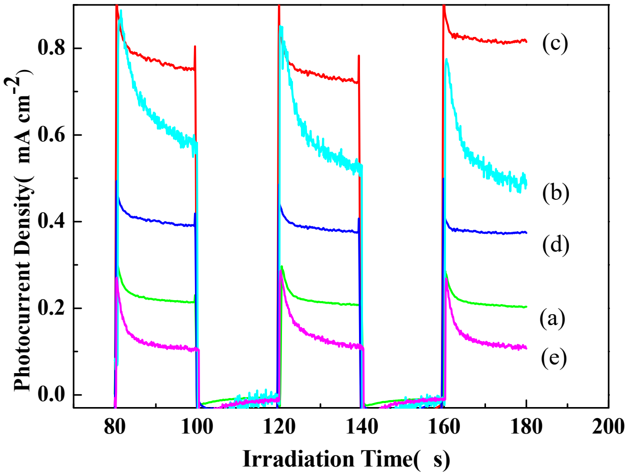

Fig. 8 Transient photoelectric response maps of (a)20s-Cu,N-TNT; (b)40s-Cu,N-TNT; (c)60s-Cu,N-TNT; (d)80s-Cu,N-TNT; (e)100s-Cu,N-TNT

It is listed that the relationship between photocurrent density and the doping time of copper of Cu,N-TNT samples in Fig.8. It is seen that the photocurrent density of Cu,N-TNT electrode increases firstly then decreases with increasing percentage composition, and reached the maximum rate when the doping time of copper is 60s (namely 60s-Cu,N-TNT). The above phenomena could result from morphological difference, namely, TNT was destroyed for 80s-Cu,N-TNT and 100s-Cu,N-TNT, which give rise to decreasing contact area between Cu,N-TNT samples and electrolyte[41, 42].

4. Conclusion

Cu,N-TNT was generated by magnetron sputtering and anodic oxidation, which has the larger absorption edge, stronger absorption intensity in visible region, less band gap than TNT. Moreover, the photocurrent density of 60s-Cu,N-TNT is large with excellent sensitivity, which could be applied widely as promising photoanode material. As a result, the present work provides a good guideline to the design of photoanode with excellent performance.

Acknowledgment

YL is grateful for the special talents science and technology innovation project of Shanxi Province of China (201705D21107).

Reference

1. Marien, C. B. D.; Cottineau, T.; Robert, D.; Drogui, P., TiO2 Nanotube arrays: Influence of tube length on the photocatalytic degradation of Paraquat. *Applied Catalysis B Environmental* **2016,** 194, 1-6.
2. Giovannozzi, A. M.; Reipa, V.; Almeida, J. L.; Cole, K. D., Electrochemical inactivation of Bacillus spores in drinking water using a quaternary oxide electrode. *Water Science & Technology Water Supply* **2011,** 11, (11), 719.
3. Lai, Y.; Tang, Y.; Gong, J.; Gong, D.; Chi, L.; Lin, C.; Chen, Z., Transparent superhydrophobic/superhydrophilic TiO2-based coatings for self-cleaning and anti-fogging. *Journal of Materials Chemistry* **2012,** 22, (15), 7420-7426.
4. Mor, G. K.; Varghese, O. K.; Paulose, M.; Shankar, K.; Grimes, C. A., A review on highly ordered, vertically oriented TiO2 nanotube arrays: Fabrication, material properties, and solar energy applications. *Solar Energy Materials and Solar Cells* **2006,** 90, (14), 2011-2075.
5. Xuan, Y.; Duan, H.; Li, Q., Enhancement of solar energy absorption using a plasmonic nanofluid based on TiO2/Ag composite nanoparticles. *Rsc Advances* **2014,** 4, (31), 16206-16213.
6. Lupan, O.; Ursaki, V. V.; Chai, G.; Chow, L.; Emelchenko, G. A.; Tiginyanu, I. M.; Gruzintsev, A. N.; Redkin, A. N., Selective hydrogen gas nanosensor using individual ZnO nanowire with fast response at room temperature. *Sensors and Actuators B: Chemical* **2010,** 144, (1), 56-66.
7. Silambarasan, D.; Surya, V. J.; Vasu, V.; Iyakutti, K., Single walled carbon nanotube-metal oxide nanocomposites for reversible and reproducible storage of hydrogen. *Acs Appl Mater Interfaces* **2013,** 5, (21), 11419-11426.
8. A. V. Emeline, §; A. V. Rudakova; V. K. Ryabchuk, ‡ and; N. Serpone, Photostimulated Reactions at the Surface of Wide Band-Gap Metal Oxides (ZrO2 and TiO2): Interdependence of Rates of Reactions on Pressure−Concentration and on Light Intensity. *Journal of Physical Chemistry B* **2015,** 102, (52), 10906-10916.
9. Alaoui, O. T.; Herissan, A.; Quoc, C. L.; Zekri, M. E. M.; Sorgues, S.; Remita, H.; Colbeau-Justin, C., Elaboration, charge-carrier lifetimes and activity of Pd-TiO 2 photocatalysts obtained by gamma radiolysis. *Journal of Photochemistry & Photobiology A Chemistry* **2012,** 242, (31), 34-43.
10. Iliev, V.; Tomova, D.; Rakovsky, S., Nanosized N-doped TiO2 and gold modified semiconductors - photocatalysts for combined UV-visible light destruction of oxalic acid in aqueous solution. *Desalination* **2010,** 260, (1), 101-106.
11. Li, Q.; Shang, J. K., Self-organized nitrogen and fluorine co-doped titanium

oxide nanotube arrays with enhanced visible light photocatalytic performance. *Environmental Science & Technology* **2009,** 43, (23), 8923-9.

12. Daghrir, R.; Drogui, P.; Robert, D., Modified TiO2 For Environmental Photocatalytic Applications: A Review. *Industrial and Engineering Chemistry Research* **2013,** 52, (10), 3581-3599.
13. Cheng, X.; Liu, H.; Chen, Q.; Li, J.; Wang, P., Preparation and characterization of palladium nano-crystallite decorated TiO_2 nano-tubes photoelectrode and its enhanced photocatalytic efficiency for degradation of diclofenac. *Journal of Hazardous Materials* **2013,** 254-255, (1), 141-148.
14. Kınacı, B.; Çetin, S. Ş.; Bengi, A.; Özçelik, S., The temperature dependent analysis of Au/TiO 2 (rutile)/n-Si (MIS) SBDs using current–voltage–temperature (I–V–T) characteristics. *Materials Science in Semiconductor Processing* **2012,** 15, (5), 531-535.
15. Hosseini, M. G.; Momeni, M. M., UV-cleaning properties of Pt nanoparticle-decorated titania nanotubes in the electro-oxidation of methanol: An anti-poisoning and refreshable electrode. *Electrochimica Acta* **2012,** 70, (6), 1-9.
16. Xin, B. F.; Jing, L. Q.; Hong Gang, F. U.; Wang, B. Q., Preparation and Characterization of Cu Doped TiO_2 Nanoparticles and Their Photocatalytic Activity. *Chemical Research in Chinese Universities* **2004,** 177, (10), 3375-3382.
17. Qiu, X.; Miyauchi, M.; Sunada, K.; Minoshima, M.; Liu, M.; Lu, Y.; Li, D.; Shimodaira, Y.; Hosogi, Y.; Kuroda, Y., Hybrid CuxO/TiO2 Nanocomposites As Risk-Reduction Materials in Indoor Environments. *Acs Nano* **2012,** 6, (2), 1609-18.
18. Montini, T.; Gombac, V.; Sordelli, L.; Delgado, J. J.; Chen, X.; Prof.; #x; Adami, D. G.; Prof.; #x; Fornasiero, D. P., Nanostructured Cu/TiO2 Photocatalysts for H2 Production from Ethanol and Glycerol Aqueous Solutions. *Chemcatchem* **2011,** 3, (3), 574–577.
19. Andrei Ghicov; †, J. M. M.; Hiroaki Tsuchiya; Julia Kunze; Volker Haeublein; Lothar Frey, A.; Patrik Schmuki, Ion Implantation and Annealing for an Efficient N-Doping of TiO2 Nanotubes. *Nano Letters* **2006,** 6, (5), 1080-1082.
20. Alotaibi, A. M.; Sathasivam, S.; Williamson, B. A. D.; Kafizas, A.; Sotelovazquez, C.; Taylor, A.; Scanlon, D. O.; Parkin, I. P., Chemical Vapor Deposition of Photocatalytically Active Pure Brookite TiO2 Thin films. *Chemistry of Materials* **2018,** 30, (4).
21. Zou, X. J.; Li, X. Y.; Qu, Z. P.; Wang, J. J., [Preparation, characterization of Si doped TiO2 nanotubes and its application in photocatalytic oxidation of VOCs]. *Huan Jing Ke Xue* **2011,** 32, (12), 3694-3698.
22. Kamarozaman, N. S.; Asiah, M. N.; Aznilinda, Z.; Bakar, R. A.; Abdullah, W. F. H.; Herman, S. H.; Rusop, M., Memristive Behavior of TiO2 Nanostructures Grown at Different Substrate Positioning by Immersion Method. *Advanced Materials Research* **2013,** 795, 256-259.
23. Kitano, M.; Funatsu, K.; Matsuoka, M.; Ueshima, M.; Anpo, M., Preparation

of nitrogen-substituted TiO2 thin film photocatalysts by the radio frequency magnetron sputtering deposition method and their photocatalytic reactivity under visible light irradiation. *Journal of Physical Chemistry B* **2006,** 110, (50), 25266-25272.

24. Seeger, S.; Ellmer, K.; Weise, M.; Gogova, D.; Abou-Ras, D.; Mientus, R., Reactive magnetron sputtering of Nb-doped TiO 2 films: Relationships between structure, composition and electrical properties. *Thin Solid Films* **2016,** 605, 44-52.
25. Teodorescu-Soare, C. T.; Dobromir, M.; Stoian, G.; Luca, D. In *Preparation of Nb-Doped TiO2 Nanotubes Using Magnetron Sputtering*, International Conference on Global Research and Education, 2017; pp 191-199.
26. Kitano, M.; Funatsu, K.; Matsuoka, M.; Ueshima, M.; Anpo, M., Preparation of nitrogen-substituted TiO2 thin film photocatalysts by the radio frequency magnetron sputtering deposition method and their photocatalytic reactivity under visible light irradiation. J Phys Chem B 110:25266. *Journal of Physical Chemistry B* **2006,** 110, (50), 25266-25272.
27. Jeon, M. K.; Park, J. W.; Kang, M., Hydrogen production from methanol/water decomposition in a liquid photosystem using the anatase and rutile forms of Cu-TiO2. *Journal of Industrial & Engineering Chemistry* **2007,** 13, (1), 84-91.
28. Song, G. B.; Liang, J. K.; Liu, F. S.; Peng, T. J.; Rao, G. H., Preparation and phase transformation of anatase–rutile crystals in metal doped TiO2/muscovite nanocomposites. *Thin Solid Films* **2005,** 491, (1), 110-116.
29. Arbiol, J.; Cerda, J.; Dezanneau, G.; Cirera, A., Effects of Nb doping on the TiO2 anatase-to-rutile phase transition. *Journal of Applied Physics* **2002,** 92, (2), 853-861.
30. Li, S.; Jena, P., Origin of the Anatase to Rutile Conversion of Metal-Doped TiO2. *Physical Review B Condensed Matter* **2009,** 79, (20).
31. Bahnemann, D.; Dillert, R.; Kandiel, T. A., Titanium Dioxide Nanoparticles and Nanostructures. *Current Inorganic Chemistry* **2012,** 2, (2), -.
32. Jeong, J. H.; Jung, D. W.; Shin, E. W.; Oh, E. S., Boron-doped TiO 2 anode materials for high-rate lithium ion batteries. *Journal of Alloys & Compounds* **2014,** 604, (29), 226-232.
33. Zhou, J.; Ren, F.; Zhang, S.; Wu, W.; Xiao, X.; Liu, Y.; Jiang, C., SiO2-Ag-SiO2-TiO2 multi-shell structures: plasmon enhanced photocatalysts with wide-spectral-response. *Journal of Materials Chemistry A* **2013,** 1, (42), 13128-13138.
34. Vijayan, B. K.; Dimitrijevic, N. M.; Wu, J.; Gray, K. A., The Effects of Pt Doping on the Structure and Visible Light Photoactivity of Titania Nanotubes. *Journal of Physical Chemistry C* **2016,** 114, (49), 21262-21269.
35. Wender, H.; Feil, A. F.; Diaz, L. B.; Ribeiro, C. S.; Machado, G. J.; Migowski, P.; Weibel, D. E.; Dupont, J.; Teixeira, S. R., Self-Organized TiO2 Nanotube Arrays: Synthesis by Anodization in an Ionic Liquid and Assessment of Photocatalytic Properties. *Acs Applied Materials & Interfaces* **2011,** 3, (4), 1359.

36. Fan, J.; Zhao, Z.; Wang, J.; Zhu, L., Synthesis of Cr,N-codoped titania nanotubes and their visible-light-driven photocatalytic properties. *Applied Surface Science* **2015,** 324, 691-697.
37. Roberts, A.; Engelberg, D.; Liu, Y.; Thompson, G. E.; Alexander, M. R., Imaging XPS investigation of the lateral distribution of copper inclusions at the abraded surface of 2024T3 aluminium alloy and adsorption of decyl phosphonic acid. *Surface & Interface Analysis* **2002,** 33, (8), 697-703.
38. Tsoncheva, T.; Issa, G.; Blasco, T.; Concepcion, P.; Dimitrov, M.; Kovacheva, D.; Atanasova, G., Silica supported copper and cerium oxide catalysts for ethyl acetate oxidation. *Journal of Colloid & Interface Science* **2013,** 404, (32), 155-160.
39. Ananpattarachai, J.; Kajitvichyanukul, P.; Seraphin, S., Visible light absorption ability and photocatalytic oxidation activity of various interstitial N-doped TiO2 prepared from different nitrogen dopants. *Journal of Hazardous Materials* **2009,** 168, (1), 253-261.
40. Sun, L.; Cai, J.; Wu, Q.; Huang, P.; Su, Y.; Lin, C., N-doped TiO2 nanotube array photoelectrode for visible-light-induced photoelectrochemical and photoelectrocatalytic activities. *Electrochimica Acta* **2013,** 108, (10), 525-531.
41. Hua, Z.; Dai, Z.; Bai, X.; Ye, Z.; Wang, P.; Gu, H.; Huang, X., Copper nanoparticles sensitized TiO2 nanotube arrays electrode with enhanced photoelectrocatalytic activity for diclofenac degradation. *Chemical Engineering Journal* **2016**.
42. HODES, G.; HOWELL, I. D. J.; PETER, L. M., ChemInform Abstract: Nanocrystalline Photoelectrochemical Cells. A New Concept in Photovoltaic Cells. *ChemInform* **2010,** 24, (4), no-no.